

# Temporal Common Trends of Topsoil Water Dynamics in a Humid Subtropical Forest Watershed

A. Ritter,\* C. M. Regalado, and R. Muñoz-Carpena

Research oriented toward understanding the hydrologic functioning of the relict “laurisilva” evergreen forests is scarce. This study focused on the analysis of temporal changes in soil water status under such humid subtropical stands and explored to what extent hydrologic fluxes may explain topsoil water dynamics. Hydrologic fluxes (potential evapotranspiration, canopy fog water dripping, and rainwater below the canopy) were computed for a 2-yr period using in situ micrometeorological measurements in the Garajonay National Park cloud forest (Canary Islands). Time domain reflectometry (TDR) data were used to characterize soil water status at 0.15- and 0.30-m depths in plots located at 1145, 1185, 1230, and 1270 m above sea level. The resulting eight daily TDR data sets were studied with dynamic factor analysis. The variability in the soil water status time series was simplified and successfully described (coefficient of efficiency = 0.717) with a single temporal trend dynamic factor model (DFM), representing unexplained variability common to all plots and monitoring depths. Comparison of DFMs with and without explanatory variables (i.e., hydrologic fluxes) indicates that unexplained variability in the observed data was partially reduced by the information provided by the hydrologic fluxes. The rainfall contribution to the soil surface, and to a lesser extent forest potential evapotranspiration, were necessary variables for describing temporal changes in topsoil water status; however, dripping fog water was found to be a negligible contributor. Dynamic factor analysis proved to be useful for studying the variability in multivariate hydrologic time series without the need of a priori detailed information about the underlying mechanisms governing soil water dynamics.

ABBREVIATIONS: AIC, Akaike's information criterion; DFA, dynamic factor analysis; DFM, dynamic factor model; TDR, time domain reflectometry; VIF, variance inflation factor.

THE GARAJONAY National Park (La Gomera, Canary Islands, Spain) was declared a World Heritage Site by the United Nations Educational, Science, and Cultural Organization in 1986. The park provides the best example of the “laurisilva,” a humid, subtropical, evergreen forest that, during the Tertiary, covered southern Europe and North Africa but then disappeared from these areas during the last ice age. Today laurisilva is a relic forest present mostly in the Macaronesian archipelagos. On La Gomera Island, evergreen forests grow on particular highly evolved soils of volcanic origin, unique in the Canary Islands (Jiménez Mendoza et al., 1990). The presence of this evergreen forest on the central plateau of La Gomera contrasts sharply with the arid ecosystems at lower elevations on the island. Traditionally, such ecosystem

differences have been attributed to the humid Mediterranean climatic conditions prevailing in the area and to the mitigation of drought periods by the incidence of wind-driven fogs (Santana Pérez, 1990). Recent work has raised questions, however, about the relative importance of fog as a source of water to the forest soil (Ritter et al., 2008).

The description and modeling of forest evapotranspiration, rainfall, and fog interception and the subsequent dripping from the canopy are essential to understanding the hydrologic functioning of the forest. Such water fluxes ultimately convey water to the soil surface. In this context, several researchers have studied throughfall and patterns of soil water content spatial distribution in soils under forest cover (Mallants et al., 1996; Schaap et al., 1997; Bruckner et al., 1999; Schume et al., 2003). Finding a direct relation between throughfall and soil water content patterns may not be straightforward (Raaijmakers et al., 2002), however, because of the complex hydraulic processes taking place at the soil–plant–atmosphere interface. Typically, topsoil moisture is sensitive to small water contributions from dripping fog or short rain showers, which can cause sharp changes in the soil water content of the A horizon (e.g., Raaijmakers et al., 2002). This may be particularly true in the studied watershed, where the existence of a highly organic hydrophobic O horizon (Regalado and Ritter, 2006) could lead to rapid bypass flow of water to deeper wettable horizons through soil cracks, biopores (made by soil fauna), or roots (Wallis and Horne, 1992).

Long-term monitoring and analysis of topsoil water content time series can lead to improved understanding of the temporal dynamics of the evergreen forest hydrology. The intrinsic

A. Ritter and C.M. Regalado, Dep. Suelos y Riegos, Instituto Canario de Investigaciones Agrarias (ICIA), Apdo. 60 La Laguna, 38200 Tenerife, Spain; R. Muñoz-Carpena, Agricultural and Biological Engineering Dep., Univ. of Florida, 287 Frazier Rogers Hall, P.O. Box 110570, Gainesville, FL 32611-0570. Received 5 Mar. 2008. The mention of trade or manufacturer names is made for information only and does not imply an endorsement, recommendation, or exclusion by ICIA–Crop Research Institute. \*Corresponding author (aritter@icia.es).

Vadose Zone J. 8:437–449  
doi:10.2136/vzj2008.0054

© Soil Science Society of America

677 S. Segoe Rd. Madison, WI 53711 USA.

All rights reserved. No part of this periodical may be reproduced or transmitted in any form or by any means, electronic or mechanical, including photocopying, recording, or any information storage and retrieval system, without permission in writing from the publisher.

variability of hydrologic processes makes it difficult, however, to identify to what extent different hydrologic fluxes contribute to the observed temporal variation in soil water content. Standard analyses that are limited to visual inspection and comparative statistics of multivariate time series may not be sufficient for substantive evaluation of such data. In contrast, physically based models of water and solute transport may be useful exploratory tools to understand the complexity of these hydrologic processes (Philip, 1991). The use of such models is not an easy task, however, since they contain parameters and processes that must be identified for each specific scenario. Hence, the success of physically based models depends strongly on the identification of parameters and the reliability of the input variables. In this context, complementary exploratory techniques are desirable for coping with the lack of information about parameters and processes, as well as the uncertainties associated with the estimation or measurement of parameters and input variables.

A novel approach for studying multivariate time series is dynamic factor analysis (DFA), originally developed for economic time series interpretation (Geweke, 1977). Classical time series techniques usually require long stationary and regularly spaced temporal data sets. Time series are usually nonstationary, however, and missing values are not infrequent, especially under unattended field monitoring conditions. Although nonstationarity may be overcome by detrending, trends may hold fundamental information necessary to explain the temporal dynamics of the investigated variables. Dynamic factor analysis is a dimensionality reduction statistical technique that can handle nonstationary, short time series. Furthermore, it allows identification of common trends between multivariate time series and their relation with selected potential explanatory variables (Zuur et al., 2003b). Unlike other statistical dimension reduction techniques, such as factor and redundancy analysis, DFA takes into account the time component. Thus, underlying hidden effects driving the temporal variation in the observed data may be detected. Such driving effects may be described by common trends (representing unexplained variability) or explanatory variables consisting of other observed time series (Zuur et al., 2003a). Dynamic factor analysis has been successfully applied in hydrology to identify common trends in groundwater levels (Márkus et al., 1999; Ritter and Muñoz-Carpena, 2006) and interactions between hydrologic variables and groundwater quality trends (Muñoz-Carpena et al., 2005; Ritter et al., 2007). Hence, DFA has been shown to be an effective tool for analyzing time-dependent hydrologic data sets, for providing information about common

trends and interactions in such hydrologic time series, and for determining if the time series are affected by the selected explanatory variables. One interesting feature of DFA is that it does not require a priori information about the underlying mechanisms governing the hydrologic processes.

The study presented here focused on the analysis of temporal changes in soil water status under a humid, subtropical, evergreen forest cover. In this context, we explored to what extent hydrologic fluxes (potential evapotranspiration, fog water, and rainfall dripping) might explain the topsoil water dynamics observed in a representative forest watershed in the Garajonay National Park. A sequential three-step exploratory procedure was performed using daily topsoil water status and micrometeorologic variables monitored during a 2-yr period: (i) visual inspection of soil water status and explanatory hydrologic-flux variable time series; (ii) application of DFA to identify common trends that represent unexplained variability in the soil water status; and (iii) inclusion of explanatory hydrologic-flux variables in the DFA to assess their influence on the temporal variation in the soil water status.

## Materials and Methods

### Experimental Site

The study was performed in a 43.7-ha watershed located at 1145 to 1270 m above sea level in the Garajonay National Park (Canary Islands, Spain) (Fig. 1). The evergreen forest vegetation in the watershed is mainly composed of broadleaf tree species (10–20 m high) of the *Laureaceae* family. On crests and upper slopes, shrubby 7- to 12-m-high wax myrtle tree heath (*Myrica faya* Ait.–*Erica arborea* L.) stands are frequent (Golubic, 2001). The watershed is northeast oriented and subject to the predominant trade winds. The influence of frequent fog results in high relative humidity (>95%) (Ritter et al., 2008). Variations in mean annual temperature measured within the watershed at different plots during the 2-yr period were small ( $13 \pm 5^\circ\text{C}$  standard

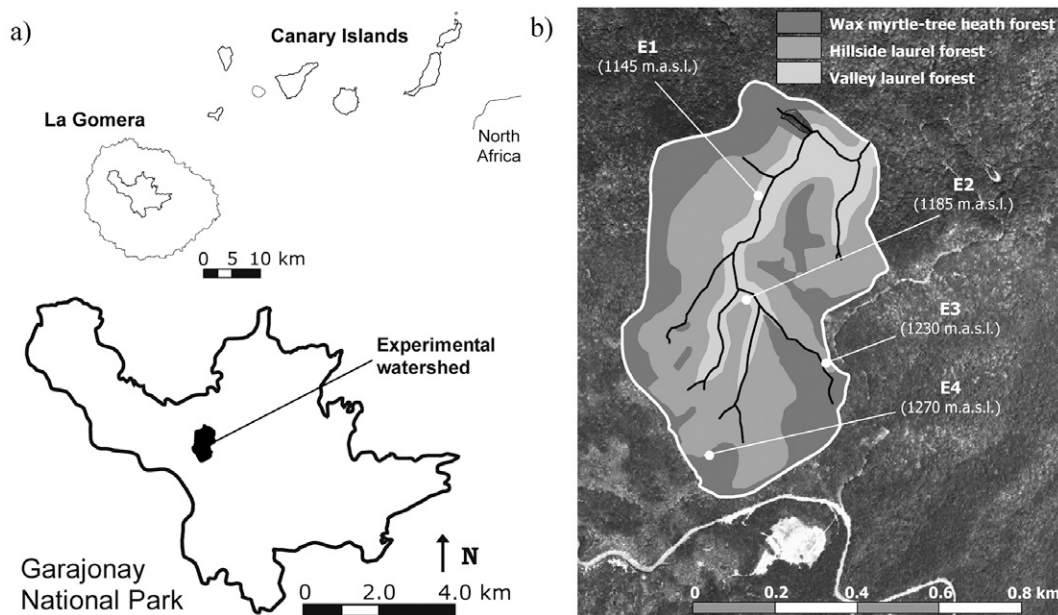


FIG. 1. (a) Location of the experimental watershed within the National Park in La Gomera (Canary Islands), and (b) distribution of plots (designated as E1, E2, E3, and E4) and subtropical evergreen forest types within the watershed. Plot elevations are given in meters above sea level (m.a.s.l.).

deviation) and mean annual precipitation was moderate (635 and 1088 mm for the first and second years, respectively). In general, soils in the national park are acidic and highly organic Andosols (Melanudands, Fulvudands, and Hapludands). These have developed over a complex geologic material composed of basaltic lava flows and successive deposits of volcanic ash. Under this humid climate, weathering of the parent material yields allophane-like noncrystalline minerals that, with incorporation of vegetation litter, produces thick, dark, humus-rich epipedons and Al- and Fe-humus complexes (Rodríguez Rodríguez et al., 2006). The soils within the watershed are classified (Soil Survey Staff, 1999) as Aluandic Andosols (Fulvudands). Their andic character is responsible for particular physicochemical and hydraulic properties, such as high permeability, low bulk density, and large microporosity and water retention capacity (Warkentin and Maeda, 1980). Four plots located at different sites within the watershed were used in this study (Fig. 1b). Each plot was selected based on its distinct elevation and vegetation type. Geographic information about these plots, together with topsoil texture, organic matter content, and pH, are shown in Table 1 and Fig. 1.

### Soil Water Status Measurements

Time domain reflectometry probes with two 0.16-m rods (Trime-EZ, Imko GmbH, Ettlingen, Germany), were inserted horizontally at 0.15- and 0.30-m soil depths at each of the four plots. The TDR measurements were collected for 2 yr (February 2003–January 2005) using a 3-min sampling frequency and averaged every 15 min with a field datalogger (Combilog, UP GmbH, Cottbus, Germany). The TDR technique is based on the transit time taken by an electromagnetic wave pulse traveling forward and backward along a transmission line (TDR rods) inserted in a sample (soil) material. It thus depends on the dielectric properties of the water–air–soil matrix composite. In the case of the Imko TDR, the pulse traveling time is obtained from voltage level comparisons at different times, and a normalized time (pseudo-transit time,  $t_p$ ) is defined. A logarithmic relationship between the dielectric constant of a material ( $\epsilon$ ) and  $t_p$  has been proposed by Regalado et al. (2006):

$$\ln(\epsilon) = 0.00478t_p + 0.34928, \quad 100 < t_p < 900 \quad [1]$$

TABLE 1. Information on the plots selected within the watershed. Soil properties correspond to the A horizon.

Plot	Elevation	Easting†	Northing†	Monitoring depth	SOM‡	pH	Texture§
	masl¶				g kg <sup>-1</sup>		
E1	1145	278,206	3,114,124	0.15	275 ± 44#	4.5 ± 0.1	scl
				0.30	186 ± 81	4.5 ± 0.0	scl
E2	1185	278,177	3,113,873	0.15	294 ± 74	4.6 ± 0.0	scl
				0.30	206 ± 50	4.5 ± 0.2	scl
E3	1230	278,371	3,113,719	0.15	318 ± 168	4.8 ± 0.1	scl
				0.30	230 ± 43	5.0 ± 0.4	sl
E4	1270	278,088	3,113,496	0.15	132 ± 30	5.1 ± 0.2	sl
				0.30	116 ± 08	5.4 ± 0.3	sl

† UTM coordinates corresponding to the 28R zone.

‡ Soil organic matter content.

§ USDA classification: scl, sandy clay loam; sl, sandy loam.

¶ m above sea level.

# Mean ± SD.

The saturation degree of a soil may be referred to in terms of its dielectric constant, obtained from Eq. [1], instead of the soil volumetric water content since this avoids the need for a soil-specific calibration and thus possible errors as a consequence of soil variability. In our case, we used the square root of the dielectric constant,  $\sqrt{\epsilon}$ , or the refractive index, as an indication of the soil water status. If required,  $\sqrt{\epsilon}$  may be related to the soil volumetric water content via an approximated form of Topp's equation (Ferré et al., 1996).

### Measurements of Hydrologic Fluxes

Hydrologic fluxes were computed to explore their effect on the topsoil water dynamics. These were the forest potential evapotranspiration ( $ET_p$ ), the rainfall contribution computed as throughfall plus canopy dripping of intercepted rainfall (pP + DP), and fog drip (DF). The methods applied to calculate these variables are described below. Wet canopy potential evaporation was computed to calculate canopy dripping as a consequence of fog and intercepted rainfall. In addition, tree transpiration was measured with a sap flow system for validating the calculated  $ET_p$  time series.

#### Wet Canopy Potential Evaporation

Wet canopy potential evaporation ( $E_p$ ) was computed from micrometeorological data collected from February 2003 to January 2005 with a 3-min sampling frequency and averaged every 15 min. Micrometeorological instruments were installed on top of a 15-m scaffolded tower in the highest elevation plot (E4, 1270 m above sea level) to measure the wind speed ( $m s^{-1}$ ) and direction ( $^\circ$ ), air temperature ( $^\circ C$ ), relative humidity (%), and solar radiation ( $W m^{-2}$ ). Micrometeorological instrumentation was further described by Ritter et al. (2008). Wet canopy potential evaporation was computed to calculate canopy dripping as a consequence of fog and rainfall. The Penman–Monteith approach (Allen et al., 1998) was used to estimate  $E_p$  at 15-min intervals:

$$E_p = \frac{(R_n - G)\Delta + \rho\kappa(e_s - e_a)/r_a}{\lambda(\Delta + \gamma)} \quad [2]$$

where  $R_n$  represents the net radiation for the vegetation cover ( $W m^{-2}$ );  $G$  is the soil heat flux ( $W m^{-2}$ ), which was approximated during daylight and nighttime periods as 10 and 50% of  $R_n$ , respectively (Allen et al., 1998);  $\Delta$  is the slope of the saturation

vapor pressure curve at ambient temperature ( $Pa K^{-1}$ );  $\rho$  is the air density ( $kg m^{-3}$ );  $\kappa$  is the heat capacity of the air ( $J kg^{-1}K^{-1}$ );  $e_s$  and  $e_a$  are the saturated and actual vapor pressures (Pa), respectively;  $r_a$  is the aerodynamic resistance ( $s m^{-1}$ );  $\lambda$  is the latent heat of vaporization ( $J kg^{-1}$ ); and  $\gamma$  is the psychrometric constant ( $Pa K^{-1}$ ). The reduction of available energy in Eq. [2] due to heat storage in the canopy was considered negligible. The aerodynamic resistance was computed after Thom (1975) and Thom and Oliver (1977):

$$r_a = \frac{4.72 \ln[(z_u - d)/z_{om}] \ln[(z_e - d)/z_{ov}]}{1 + 0.536u_z} \quad [3]$$

where  $z_u$  and  $z_e$  are the height at which the wind speed ( $u_z$  in  $\text{m s}^{-1}$ ) and relative humidity were measured, respectively. The zero plane displacement was assumed  $d = 2h/3$  with  $h$  (m) being the average height of the canopy. The vapor roughness length was estimated from  $z_{ov} = 0.1z_{om}$ , with the momentum roughness length of the forest  $z_{om} = 0.123h$  (Thom, 1971; Brutsaert, 1975). Net radiation was computed from the solar radiation data as the difference between the incoming net shortwave and the net outgoing longwave radiation (Allen et al., 1998). An albedo of 0.14 (Aschan, 1998) was chosen, which is close to the value of 0.11 proposed by Matthews (1984) for evergreen subtropical forests.

### Forest Potential Evapotranspiration

The forest potential evapotranspiration ( $ET_p$ ) at Plot E4 was calculated at 15-min intervals using a form of Eq. [2] where the psychrometric constant ( $\gamma$ ) was replaced by a modified psychrometric constant ( $\gamma^*$ ) that is dependent on the relation between the canopy surface resistance ( $r_c$ ,  $\text{s m}^{-1}$ ) and aerodynamic resistance,  $r_a$ , such that  $\gamma^* = \gamma(1 + r_c/r_a)$  (Allen et al., 1998). The  $r_c$  was considered to vary with the stomata response to environmental factors. According to Jarvis (1976) and Stewart (1988), the leaf stomata resistance ( $r_{s_{\min}} \leq r_s \leq r_{s_{\max}}$ ) may be estimated as the product of the minimum resistance,  $r_{s_{\min}}$  (i.e., the inverse of the maximum conductance corresponding to optimal conditions), times various stress functions, which vary with global radiation,  $R_g$ , leaf temperature,  $T_l$ , and relative humidity. Lhomme et al. (1998) showed that the effect of a vapor pressure deficit on stomata conductance was indirect. Thus taking into account the first two variables,  $R_g$  and  $T_l$  only,  $r_c$  may be computed as

$$r_c = \frac{r_s}{\text{LAI}_{\text{act}}} = \frac{r_{s_{\min}}}{\text{LAI}_{\text{act}}} \Psi_1^{-1}(R_g) \Psi_2^{-1}(T_l) \quad [4]$$

where  $\text{LAI}_{\text{act}}$  is the active leaf area index, computed from the leaf area index ( $\text{LAI} = 4.2$  (Golubic, 2001), reduced by a shelter factor of 1.25 (Dingman, 2002), such that  $\text{LAI}_{\text{act}} = 3.36$ . The  $\Psi_i$  ( $i = 1, 2$ ) are functions accounting for the effects of global radiation and leaf temperature on stomata conductance. Stomata conductance was measured in the laboratory with a portable photosynthesis system (LCpro, ADC BioScientific Ltd., Hoddesdon, UK) in small potted plants of different laurisilva species. The measured  $r_{s_{\min}}$  was  $137 \text{ s m}^{-1}$ . The following dependence of the stomata conductance with global radiation at optimum temperature was obtained ( $r^2 = 0.994$ ):

$$\Psi_1(R_g) = 1.02 \left[ 1 - \exp\left(-\frac{R_g - 77.35}{400.37}\right) \right]^{0.60} \quad [5]$$

$R_g > 77.35 \text{ W m}^{-2}$

$$\Psi_1(R_g) = 0 \quad [5]$$

$R_g \leq 77.35 \text{ W m}^{-2}$

For the temperature dependence of conductance, a Pearson type function was fitted to conductance vs. leaf surface temperature data pairs at saturating light conditions ( $r^2 = 0.771$ ):

$$\Psi_2(T_l) = 0.95 \left[ 1 + 0.76(T_l - 22.17)^2 \right]^{-0.51} \quad [6]$$

For the sake of simplicity,  $T_l$  ( $^{\circ}\text{C}$ ) was assumed equal to ambient temperature, although a complex dependence is expected (ADC BioScientific Ltd., 2004).

Forest-ground evaporation was assumed negligible because of the mulching effect of the 5-cm leaf litter layer covering the soil surface and the solar radiation attenuation due to the relatively dense canopy (Aschan et al., 1994).

### Tree Sap Flow Rate

Sap flow was measured on trees located in the highest elevation plot (E4, 1270 m above sea level) with Granier's heat dissipation technique (Granier, 1985) for a selected period (April 2003–October 2003). The sap flow system (SFS-2, UP GmbH, Cottbus, Germany) consists of two cylindrical needle-like probes (20-mm length and 2-mm diameter), which are inserted in the trunk. The upper probe is continuously heated with a resistor, whereas the lower probe is unheated; the resulting temperature difference,  $\Delta T$ , is measured with a thermocouple (see Regalado and Ritter [2007] for further details).

An empirical relation between sap flux density,  $q$  ( $\text{kg m}^{-2} \text{ s}^{-1}$ ), and  $\Delta T$  may be derived from Granier (1985):

$$q = 0.119 \left( \frac{\Delta T_{\text{max}}}{\Delta T} - 1 \right)^{1.231}, \quad \Delta T_{\text{max}} \geq \Delta T \quad [7]$$

The tree sap flow rate,  $Q_{\text{SF}}$  ( $\text{kg s}^{-1}$ ), was obtained from the integration of Eq. [7] in the trunk radial direction,  $r$  (m), within the conducting sapwood radial interval ( $r_h$ ,  $r_x$ ):

$$Q_{\text{SF}} = 2\pi \int_{r_h}^{r_x} r q_l(r) dr \quad [8]$$

where  $q_l(r)$  is the sap flux density at the radial depth  $l$ , and  $r_h$  and  $r_x$  are the radii at the heartwood and the cambium, respectively. We derived polynomial expressions for  $q_l(r)$  from radial patterns of sap flow distribution reported by Jiménez et al. (2000) in laurel forest tree species.

### Rainfall Contribution to the Soil Surface

Rainfall water may reach the soil surface as both throughfall precipitation,  $pP$  (mm), and canopy dripping,  $DP$  (mm), which is a consequence of the water intercepted by the vegetation. The interception process was described with the Rutter et al. (1971) approach, whereby the interception losses were computed from a water balance at both the stand and stem levels. This model considers that water stored in the canopy changes with time according to the following continuity equation:

$$\frac{\Delta S}{\Delta t} = I - E - D \quad [9]$$

where  $\Delta S/\Delta t$  is the rate of change in stored water ( $\text{mm min}^{-1}$ ),  $I$  is the interception rate by the canopy ( $\text{mm min}^{-1}$ ),  $E$  is the wet canopy evaporation rate ( $\text{mm min}^{-1}$ ), and  $D$  is the dripping rate ( $\text{mm min}^{-1}$ ). The term  $I$  is given by

$$I = \frac{P}{\Delta t}(1 - p_t - p) \quad [10]$$

where  $P$  is the precipitation (mm) measured with a Rain-O-Matic Professional spoon tipping rain gauge (Pronamic Bekhoi International Trading Engineering Co. Ltd., Silkeborg, Denmark) placed above the canopy;  $p_t$  ( $\text{m m}^{-1}$ ) is the precipitation fraction that is diverted toward the stems (stemflow); and  $p$  ( $\text{m m}^{-1}$ ) is the throughfall or rainfall fraction that passes through the stand and reaches the ground without being intercepted. In this study, we used  $p_t = 0.0164 \text{ m m}^{-1}$  computed from the values for *Erica arborea* L., *Myrica faya* Ait., and *Laurus azorica* (Seub.) Franco obtained by Aboal et al. (1999) in the Agua García evergreen forests (Tenerife, Canary Islands). The value  $p = 0.0805 \text{ m m}^{-1}$  was computed from van Dijk and Bruijnzel (2001), taking LAI = 4.2 and an extinction coefficient equal to 0.6. This value is similar to the value of  $p = 0.092 \text{ m m}^{-1}$  obtained by Aboal (1998) in the Agua García evergreen forests.

According to Eq. [9], a fraction of the intercepted water is lost by evaporation. Following Rutter et al. (1971), the wet canopy evaporation rate is proportional to the volume stored in the canopy:

$$E = E_p \frac{S}{S_{\max}}, \quad S \leq S_{\max} \quad [11]$$

where  $S_{\max}$  (mm) is the maximum canopy storage capacity. When water intercepted by the canopy exceeds  $S_{\max}$ , it drips according to the following exponential function:

$$D = D_s \exp[b(I\Delta t - S_{\max})] \quad [12]$$

where  $D_s$  ( $\text{mm min}^{-1}$ ) and  $b$  (unitless) are empirical parameters. Gash and Morton (1978) have suggested that  $D_s$  and  $b$  may be taken from Rutter et al. (1971). Nevertheless, it is advisable to make a correction to take into account an appropriate LAI or  $S_{\max}$  (Rutter et al., 1975; Aboal, 1998). Consequently, the following values were used in this study:  $D_s = 2.31 \times 10^{-3} \text{ mm min}^{-1}$  and  $b = 4.281$ . The maximum canopy storage capacity of the forest was computed following the method proposed by Leyton et al. (1967). Their method uses only rainfall events (preceded by 24 h with no rain) when precipitation is sufficient to saturate the canopy (e.g.,  $P > 2 \text{ mm}$ ). For these events, rainfall measured above the stand was plotted against water collected by eight gauges placed below the canopy. A line with slope  $(1 - p_t)$  is fitted such that the  $y$  axis intercept corresponds to  $S_{\max}$ . The application of the Leyton et al. (1967) method was performed using 12-h accumulated rainfall events rendering  $S_{\max} = 1.215 \text{ mm}$ .

Analogous to the equations at the stand level described above, the water balance at the stems was computed by applying Eq. [9] with the following assumptions, where the  $t$  subscripts refer to stem-related variables: the water reaching the stems is given by  $I_t = p_t P$ ; the dripping rate was assumed to be instantaneous (i.e.,  $D_t = S_t - S_{t_{\max}}$ ,  $S_t > S_{t_{\max}}$ ), where the stem maximum storage capacity ( $S_{t_{\max}} = 0.08 \text{ mm}$ ) was taken from Aboal (1998). Thereby, the amount of intercepted rainfall dripping onto the soil surface was computed as  $DP = (D + D_t)\Delta t$ . Finally, the evaporation rate,  $E_t$ , is similar to Eq. [11], and the potential evaporation rate,  $E_{pt}$ , was assumed to be 10% of  $E_p$ .

Similarly, dripping from the canopy and stems as a consequence of fog water intercepted by the vegetation, DF, was computed as described above for those periods where fog precipitation occurred and no rainfall was observed. Hence, Eq. [10] simplifies to  $I = F$ , where  $F$  ( $\text{mm min}^{-1}$ ) is the fog water collected by the canopy. The  $F$  value was estimated by combining the fog-catcher measurements made on top of the micrometeorological instrument tower and a physically based impaction model (Ritter et al., 2008).

### Dynamic Factor Analysis

The soil water status time series obtained with TDR were investigated using DFA. Dynamic factor analysis is a parameter optimization technique, and therefore it may be useful for finding interactions between time-series response and explanatory variables that are different in nature or are not related in a straightforward manner (Zuur et al., 2003a). This means that a detailed description about how the soil water status (response time series) and the hydrologic fluxes (explanatory variables) interact is not required when using DFA to evaluate how the latter influence the soil water dynamics. Compared with physically based simulation models, this DFA feature is relevant for the study presented here. In this context, we used DFA to simultaneously examine the soil water status measured at different locations that might be affected by different vegetation types, soil surface conditions, and differences in soil hydraulic properties. In addition, taking into account that uncertainty associated with soil-specific calibrations may introduce errors in the data, DFA allowed us to relate the aboveground hydrologic fluxes and the soil water dynamics expressed in terms of the refractive index ( $\sqrt{\epsilon}$ ), instead of using volumetric moisture derived from TDR laboratory calibrations.

### The Dynamic Factor Model

Dynamic factor analysis is based on the structural time series models (Harvey, 1989). A DFM serves as a description of the time-dependent series of measured data of  $N$  response variables such that (Lütkepohl, 1991; Zuur et al., 2003a)

$$N \text{ time series} = \text{linear combination of } M \text{ common trends} + \text{level parameter} + K \text{ explanatory variables} + \text{noise} \quad [13]$$

Keeping the number of  $M$  common trends as small as possible is desirable because it eases interpretation of the fitted trends. The inclusion of  $K$  explanatory variables, when readily available, is also advisable. The multilinear model in Eq. [13] may be written in mathematical form as

$$\mathbf{s}_n(t) = \sum_{m=1}^M \gamma_{m,n} \boldsymbol{\alpha}_m(t) + \mu_n + \sum_{k=1}^K \beta_{k,n} v_k(t) + \varepsilon_n(t) \quad [14]$$

$$\boldsymbol{\alpha}_m(t) = \boldsymbol{\alpha}_m(t-1) + \boldsymbol{\eta}_m(t) \quad [15]$$

where  $\mathbf{s}_n(t)$  is the size  $N$  ( $1 \leq n \leq N$ ) vector containing the values of the response variables at time  $t$ . In this study,  $N$  represents the eight temporal time series of topsoil TDR data (i.e., the soil refractive index,  $\sqrt{\epsilon}$ , for the 0.15- and 0.30-m depths at the four plots);  $\boldsymbol{\alpha}_m(t)$  is a length  $M$  ( $1 \leq m \leq M$ ) vector containing the

common unknown trends at time  $t$ ;  $\gamma_{m,n}$  are the factor loadings or weighting coefficients for each  $\alpha_m(t)$  trend; the constant-level parameter  $\mu_n$  shifts each linear combination of common trends up or down;  $\beta_{k,n}$  represents the fitted regression parameters for the  $k$ th (for  $1 \leq k \leq K$ ) explanatory variable  $v_k(t)$ ;  $K$  corresponds here to the number of hydrologic fluxes considered in the DFA;  $\varepsilon_n(t)$  and  $\eta_m(t)$  are (independent) Gaussian distributed noise with zero mean and unknown diagonal covariance matrix. Parameters  $\gamma_{m,n}$  and  $\mu_n$  in Eq. [14–15] were searched with the expectation maximization algorithm (Dempster et al., 1977; Shumway and Stoffer, 1982; Wu et al., 1996). The  $\alpha_m(t)$  trends were modeled as a random walk (Harvey, 1989) and were estimated using the Kalman filter/smoothing algorithm and the expectation maximization method, while the regression parameters associated with the explanatory variables ( $\beta_{k,n}$ ) were modeled as in linear regression (Zuur and Pierce, 2004). Dynamic factor analysis was implemented using the Brodgar Version 2.5.6 statistical package (Highland Statistics Ltd., Newburgh, UK). Further details about DFA may be found in Zuur et al. (2003a,b, 2007).

The size of the weighting factors accompanying both trends and explanatory variables ( $\gamma_{m,n}$  and  $\beta_{k,n}$ , respectively) permitted us to identify relevant soil water status time trends and responsible hydrologic components. In other words, the results from the DFA may be interpreted in terms of the canonical correlation coefficients  $\rho_{m,n}$ , the regression parameters  $\beta_{k,n}$  and the match between modeled and observed  $s_n(t)$  values. The performance of the DFM was quantified with both the coefficient of efficiency ( $-\infty \leq C_{\text{eff}} \leq 1$ , Nash and Sutcliffe, 1970) and Akaike's information criterion (AIC; Akaike, 1974). For two different DFMs, the DFM with the largest  $C_{\text{eff}}$  and smallest AIC is preferred. Additionally, cross-correlation between the  $s_n(t)$  response variables and the  $\alpha_m(t)$  common trends was quantified by means of the  $\rho_{m,n}$  canonical correlation coefficients, such that a  $\rho_{m,n}$  close to unity indicates that the corresponding common trend is highly associated with the response variable. In the following, we will refer to correlation between  $s_n(t)$  and  $\alpha_m(t)$  as being minor when  $|\rho_{m,n}| < 0.30$ , low when  $0.30 \leq |\rho_{m,n}| < 0.50$ , moderate when  $0.50 \leq |\rho_{m,n}| \leq 0.75$ , and high when  $|\rho_{m,n}| > 0.75$ . Finally, the weights of the  $k$ th explanatory variable  $v_k$  on each  $s_n(t)$  are given by the regression parameters,  $\beta_{k,n}$ . The magnitude of the  $\beta_{k,n}$  and their associated standard errors were used to assess with a  $t$ -test whether response and explanatory variables were significantly related ( $t$  value  $> 2$ ).

The DFA was performed sequentially, such that the number of  $M$  common trends was varied until a minimum AIC was achieved (Zuur et al., 2003b). Once a minimum  $M$  was identified, different combinations of explanatory variables were incorporated in the analysis until a satisfactory combination of common trends and explanatory variables was found. By including explanatory variables into the DFM, one may expect to reduce the unexplained variability and improve the description of the topsoil water time variability.

### Seasonality in the Time Series

Before the analysis, one may look for seasonality in the TDR time series (expressed as the soil refractive index,  $\sqrt{\varepsilon}$ ). Removal of the data seasonal component is convenient (Zuur and Pierce, 2004). Seasonality may be identified as periodic patterns either in the mean and/or the variance of  $\sqrt{\varepsilon}$  monthly values. Among different methods for deseasonalizing, a simple one is seasonal

standardization (Salas, 1993), whereby the monthly mean ( $\bar{s}_{n,j}$ ) and standard deviation ( $\sigma_{n,j}$ ) components are removed from the original data set such that

$$s_{n,j}^* = (s_{n,j} - \bar{s}_{n,j}) / \sigma_{n,j} \quad [16]$$

where  $s_{n,j}$  is the  $s_n$  TDR data subset corresponding to the  $j$ th month, and  $s_{n,j}^*$  is the corresponding deseasonalized time series.

### Explanatory Variables in the Dynamic Factor Model

To assess the relative effect of the hydrologic fluxes on the temporal variation in soil water status (expressed as  $\sqrt{\varepsilon}$ ), the fluxes can be included in the DFA as explanatory variables. It may be noticed that while actual TDR data at time  $t$ ,  $s_n(t)$ , are related to previous values,  $s_n(t-1)$ , this is not the case for the hydrologic fluxes, where, for instance, precipitation measured at time  $t$  does not contain information about antecedent ( $t-1$ ) rainfall events. To incorporate such a "memory feature" into the explanatory variables, one may introduce the hydrologic fluxes into the DFM as cumulative time series. This approach may, however, result in multicollinearity between the explanatory variables, which would bias the DFA. The severity of such a multicollinearity may be detected by computing the corresponding variance inflation factors (VIFs) for each explanatory variable (Zuur et al., 2007). On the other hand, on a water budget basis, input and output fluxes across the soil surface are responsible for changes in the soil water status. Thus, alternatively, the analysis of the  $s_n$  time series may be conducted using daily increments instead of actual  $\sqrt{\varepsilon}$  values. Multicollinearity may also arise between different explanatory variables measured at nearby locations, as is probably the case for the selected hydrologic fluxes measured at different plots within the watershed. Using explanatory variables measured at the four plots would thus provide redundant information for the DFA due to multicollinearity. Therefore, only those explanatory variables measured at Plot E4 were used in the DFA: forest potential evapotranspiration ( $ET_p$ ), rainfall contribution to the soil surface (pP + DP), and intercepted fog water dripping from the canopy (DF). While (pP + DP) and DF are considered soil surface water inputs,  $ET_p$  is related to tree water uptake from the root zone and it represents a soil water output. As was done with the response  $\sqrt{\varepsilon}$  time series, the seasonal component observed in the explanatory variables was removed by seasonal standardization. Additionally, those explanatory variables exhibiting no seasonality were normalized to facilitate interpretation and comparison of the regression parameters (Zuur et al., 2003b; Zuur and Pierce, 2004) resulting from the DFA.

## Results and Discussion

### Visual Exploratory Analysis of Experimental Time Series

Figure 2 shows the 2-yr observed daily variation for the three hydrologic fluxes determined for Plot E4 and the soil refractive index measured at the four plots. Visual inspection of the eight  $\sqrt{\varepsilon}$  time series (Fig. 2d) suggests the existence of common trends in  $\sqrt{\varepsilon}$ , but differences between plots and depths are also observed. It is noted that for Plots E1, E2, and E4,  $\sqrt{\varepsilon}$  time series at 0.15 and 0.30 m exhibit similar dynamics. In contrast, at Plot E3, a relative

lack of  $\sqrt{\epsilon}$  change is observed at the 0.30-m depth from October 2003 through June 2004; however,  $\sqrt{\epsilon}$  shows marked changes at Plot E3 in the upper monitoring depth. The  $\sqrt{\epsilon}$  dynamics at E1 are smoother than those observed at the other three plots. The reasons for the differences observed among plots and depths are not clear, but may be related to soil heterogeneity, differences in soil surface conditions, preferential flow, the influence of vegetation type, etc. In general, soil water dynamics at the four plots and at both monitoring depths (0.15 and 0.30 m) exhibited higher  $\sqrt{\epsilon}$  values during October to June (the rainy period), which decreased progressively to lower  $\sqrt{\epsilon}$  during July to September (the dry period). Soil wetting and drying at the 0.15-m depth were markedly reflected in the 0.15-m soil depth data, with sharp  $\sqrt{\epsilon}$  changes during precipitation events. The amount of rainfall reaching the soil surface (i.e., the sum of throughfall and intercepted rainfall dripping from the canopy) followed a cyclic pattern of wet (October–June) and dry months (July–September) (Fig. 2a). In contrast, the amount of intercepted fog water dripping from the canopy (DF) was more evenly distributed during the measurement period (Fig. 2b). Potential evapotranspiration ( $ET_p$ ) was generally greatest during the dry period and least during the rainy period (Fig. 2c). Penman–Monteith  $ET_p$  was compared with the tree sap flow rate ( $Q_{SF}$ ) to assess whether the  $ET_p$  and tree transpiration trends were consistent. Figure 3 illustrates the evolution of  $ET_p$  and  $Q_{SF}$  for a selected tree from April until October 2003, and shows good agreement in the temporal patterns exhibited by the two variables, with a cross-correlation coefficient of 0.87. The corresponding patterns in  $ET_p$  and  $Q_{SF}$  indicated that plant water uptake was never limited, possibly due to root water availability and uptake at depths below 0.30 m. Water uptake from greater depths is supported by a soil survey of the watershed (Thissen, 2001) that documented abundant roots down to a depth of 1.15 m. Yearly totals for  $pP + DP$ ,  $DF$ , and  $ET_p$  at Plot E4 were

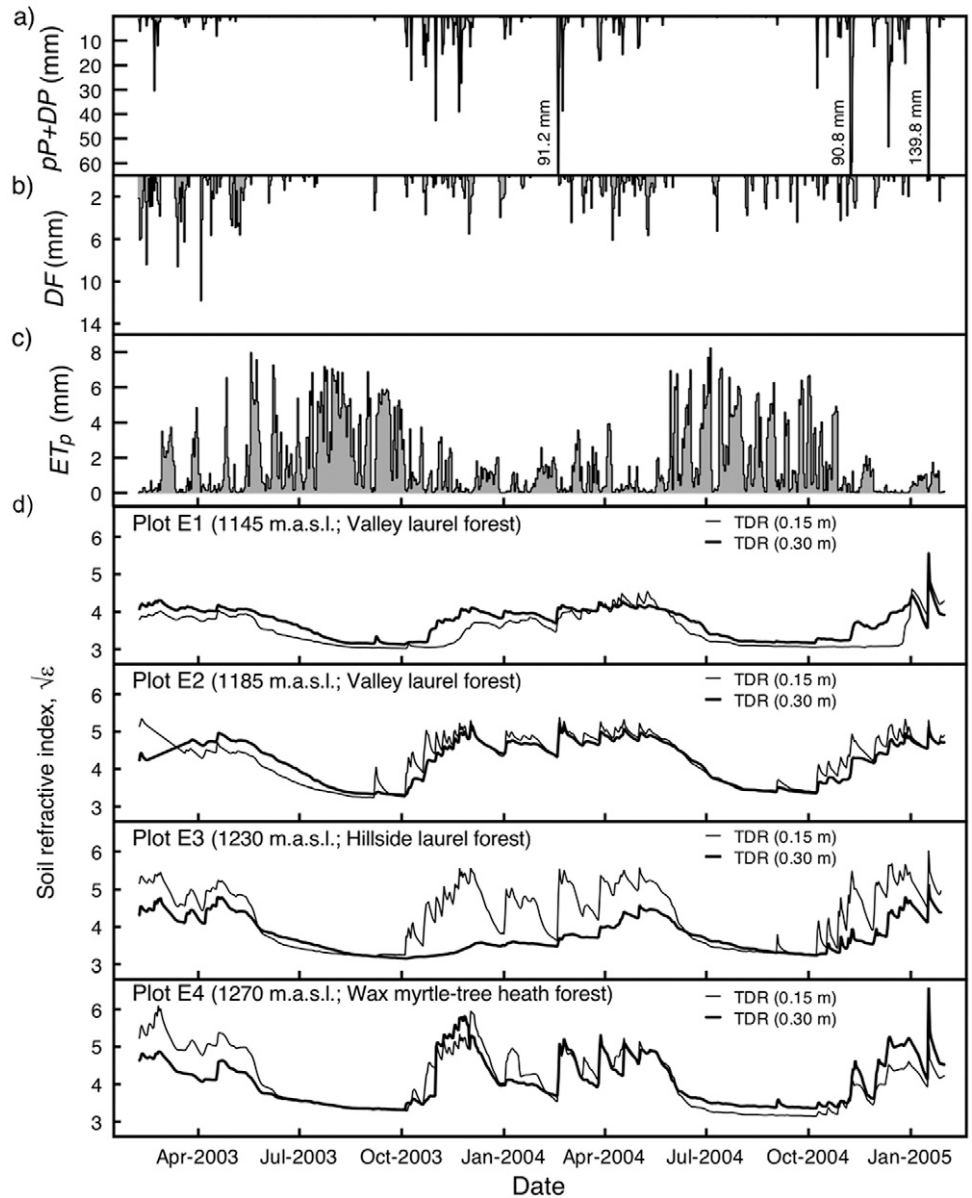


FIG. 2. Evolution of observed daily hydrologic fluxes at Plot E4: (a) rainfall contribution to the soil surface as the sum of throughfall (pP) and canopy drip (DP); (b) intercepted fog water dripping from the canopy (DF); and (c) potential evapotranspiration ( $ET_p$ ); (d) evolution of measured daily soil water content (expressed as the soil refractive index,  $\sqrt{\epsilon}$ ) determined by time domain reflectometry (TDR) at 0.15- and 0.30-m depths in the four plots within the watershed. Plot elevations are given in meters above sea level (m.a.s.l.).

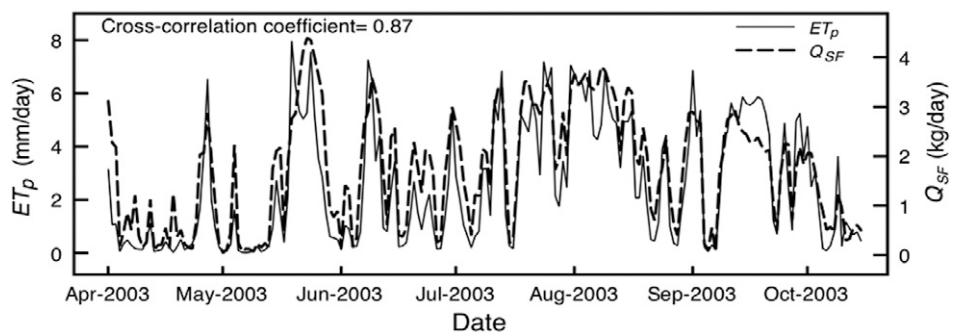


FIG. 3. Evolution of daily potential evapotranspiration ( $ET_p$ ) and tree sap flow rate ( $Q_{SF}$ ) for a selected period (April 2003–October 2003) at Plot E4.

451, 227, and 629 mm (February 2003–January 2004) and 886, 166, and 568 mm (February 2004–January 2005), respectively. In conclusion, soil water status exhibits physically reasonable responses, which may be qualitatively explained by the observed hydrologic fluxes. Following the visual exploratory analysis, DFA was used to gain insight into the relative contribution of the hydrologic fluxes to the dynamics of the soil water time series.

## Dynamic Factor Analysis

### Response and Explanatory Variables

As discussed above, seasonality was observed in the  $ET_p$  and eight  $\sqrt{\epsilon}$  temporal series, such that seasonal standardization was conducted before the DFA to remove the seasonal component. The deseasonalized time series for these two variables are denoted here as  $\sqrt{\epsilon^*}$  and  $ET_p^*$ , respectively. In contrast,  $pP + DP$  and  $DF$  did not exhibit a clear periodic pattern, but they were normalized to facilitate the interpretation of the DFA results. Normalization of  $pP + DP$  and  $DF$  was accomplished by subtracting their respective mean and dividing by their standard deviation. The resulting transformed time series, denoted here as  $(pP + DP)^*$  and  $DF^*$ , are thus zero centered, have unit variance, and are unitless. From a hydrologic point of view, the soil-water-status response variable may be related to the explanatory hydrologic-flux variables using two different approaches: (i) by relating instantaneous  $\sqrt{\epsilon^*}$  to cumulative daily total values of the hydrologic fluxes or (ii) by relating daily changes in  $\sqrt{\epsilon^*}$  (defined as  $\Delta\sqrt{\epsilon^*}$ ) to discrete

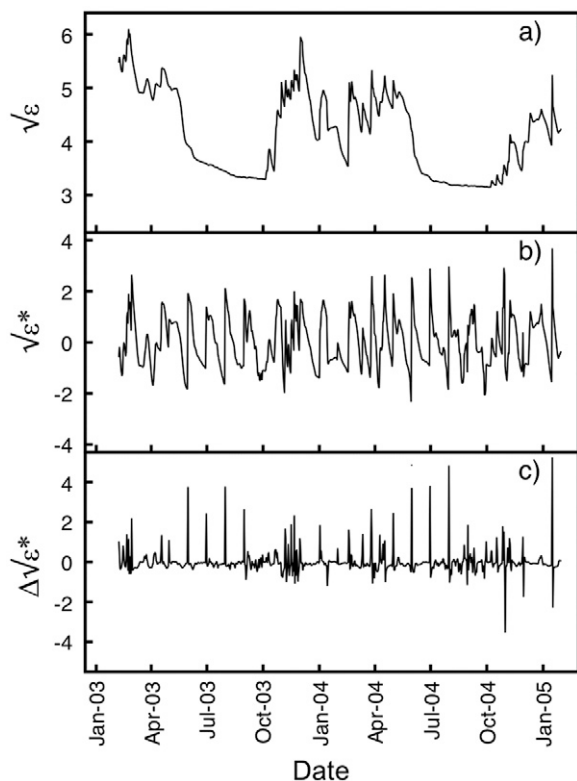


FIG. 4. Examples of time series of the (a) untransformed soil refractive index ( $\sqrt{\epsilon}$ ), (b) the deseasonalized  $\sqrt{\epsilon}$  ( $\sqrt{\epsilon^*}$ ), and (c) daily changes in  $\sqrt{\epsilon^*}$  ( $\Delta\sqrt{\epsilon^*}$ ) for Plot E4 at the 0.15-m depth. The dynamic factor analyses for this study were done using  $\Delta\sqrt{\epsilon^*}$  transformed values and discrete daily total hydrologic flux values.

daily total values of the hydrologic fluxes (see above). The former approach was abandoned after verifying the existence of multicollinearity among the explanatory variables expressed as cumulative daily totals (VIFs > 5). In contrast, evidence of multicollinearity was greatly reduced for the latter approach (VIFs < 1.2). Thus, the DFA reported here was ultimately done using  $s_n = \Delta\sqrt{\epsilon^*}$  and discrete daily total hydrologic flux values. Figure 4 illustrates the effect of applying the  $\sqrt{\epsilon^*}$  and  $\Delta\sqrt{\epsilon^*}$  transformations to the Plot E4, 0.15-m-depth response variable.

### Common Trends in Soil Water Status

The DFA is based on modeling the observed  $\Delta\sqrt{\epsilon^*}$  response time series in terms of several components. Various DFMs were formulated, differing in the number of common trends and explanatory variables used (Table 2). Evaluation of the  $C_{eff}$  and AIC statistics indicates first that, when no explanatory variables ( $K = 0$ ) are considered, the DFM that best described the eight response time series with a minimal number of common trends is that defined by one common trend ( $M = 1$ , AIC = 5869,  $C_{eff} = 0.717$ ). The inclusion of additional trends in the DFMs resulted in slightly higher  $C_{eff}$ , but also higher AICs (Table 2). Hence, the variation observed in the soil refractive index at the two monitoring depths in the four plots may be described by a single trend shown in Fig. 5a. This trend illustrates the variability, which is common to all time series. It may be viewed as a “black box” accounting for the soil properties and physical processes (soil surface water inputs and outputs, water flow in the entire soil profile, etc.) involved in the soil water dynamics. Thus, the common trend may be interpreted solely as unexplained variability. Although yet unexplained, the DFA suggests that the contribution and interactions of these effects are common to all response time series regardless of the depth and monitoring location within the watershed. To what extent each response time series is influenced by this common trend is quantified by the canonical correlation coefficients ( $\rho_{1,n}$ ) shown in the right panel in Fig. 5a. The common trend exhibited high positive correlations ( $\rho_{1,n} > 0.8$ ) with all response time series for Plots E2, E3, and E4 and moderate correlations with those  $\Delta\sqrt{\epsilon^*}$  for Plot E1.

TABLE 2. Selection of dynamic factor models (DFM) based on performance coefficients (Akaike’s information criterion [AIC] and the coefficient of efficiency [ $C_{eff}$ ]). Italicized numbers indicate the best DFM for each type, with and without explanatory variables.

Explanatory variables†	Common trends	AIC‡	$C_{eff}$ §
None	1	5869	0.717
None	2	5932	0.800
None	3	5954	0.799
$ET_p^*$ , $(pP + DP)^*$	1	5702	0.719
$ET_p^*$ , $DF^*$	1	5842	0.719
$ET_p^*$	1	5852	0.718
$(pP + DP)^*$	1	5711	0.718
$ET_p^*$ , $(pP + DP)^*$ , $DF^*$	1	5691	0.720
$ET_p^*$ , $(pP + DP)^*$ , $DF^*$	2	5745	0.800

†  $ET_p^*$ , seasonally standardized potential evapotranspiration;  $(pP + DP)^*$ , standardized rainfall contribution to the soil surface as the sum of throughfall and canopy drip;  $DF^*$ , standardized intercepted fog water dripping from the canopy.

‡ The lowest number represents the best model.

§ Computed with the combined set of predicted vs. observed values for the eight daily change in the deseasonalized soil refractive index ( $\Delta\sqrt{\epsilon^*}$ ) time series.

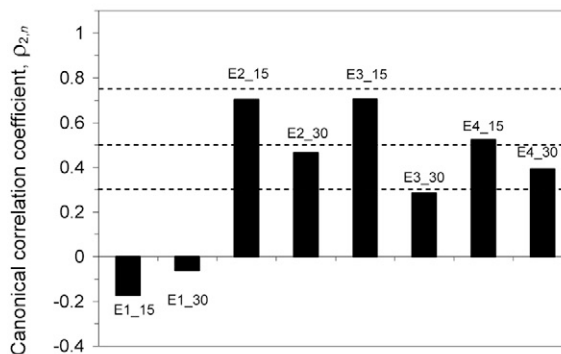
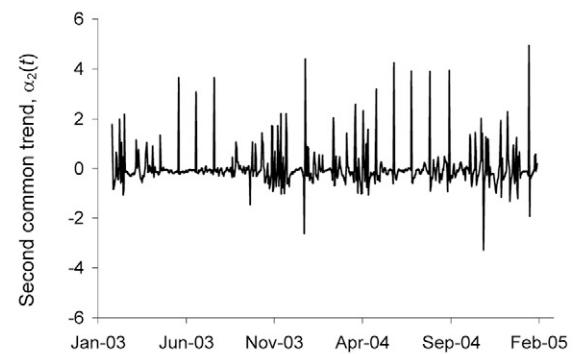
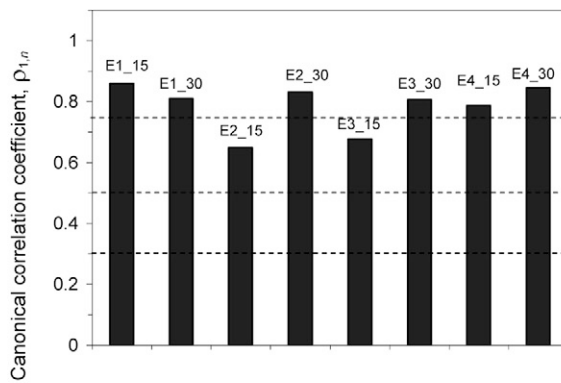
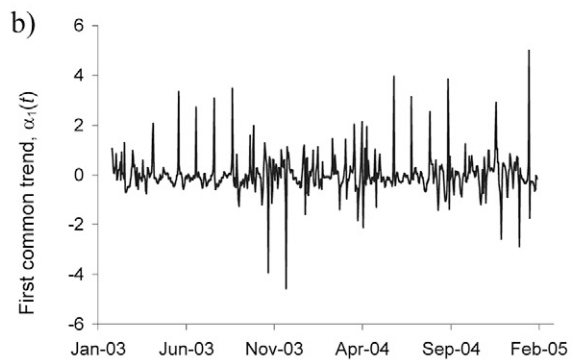
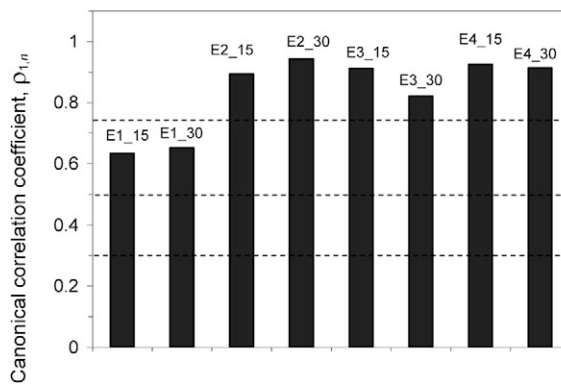
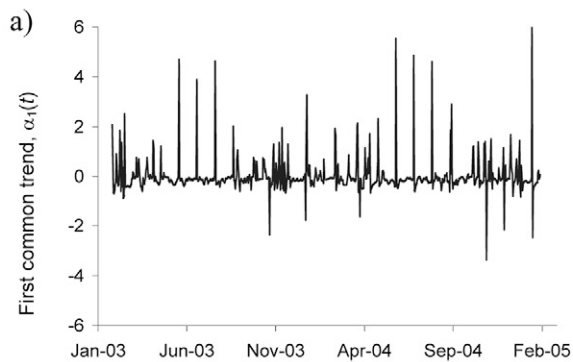


FIG. 5. Common trends and associated canonical correlation coefficients ( $\rho_{m,n}$ ) for the dynamic factor model without explanatory variables ( $K = 0$ ) and (a) one common trend and (b) two common trends. The E#\_## notation represents the plot number and measurement depth identifier (e.g., E1\_15 corresponds to Plot E1 at the 0.15-m depth). Dashed lines in the right panels delimit minor ( $|\rho_{m,n}| < 0.30$ ), low ( $0.30 \leq |\rho_{m,n}| < 0.50$ ), moderate ( $0.50 \leq |\rho_{m,n}| \leq 0.75$ ), and high ( $|\rho_{m,n}| > 0.75$ ) correlation bounds.

Additionally, Fig. 5b illustrates the DFA results after including an additional trend. The first common trend was important for explaining all response time series ( $\rho_{1,n} > 0.65$ ), and the second one complements the description of these, especially of Plots E2 and E3 at 15-cm depth, which showed moderate correlations ( $\rho_{1,n} < 0.75$ ) with the first trend. Performing the DFA with a second trend increases the degrees of freedom of the DFM and thereby improves its goodness of fit ( $C_{\text{eff}}$  of 0.717 vs. 0.800), but the penalty for inclusion of the additional parameters is an increase in the AIC (5869 vs. 5932) (Table 2). This DFM with two common trends may be viewed as a way to split the unexplained variability; however, the simpler  $M = 1$  DFM model was preferred.

#### Relative Contribution of Hydrologic Fluxes

In an attempt to reduce the unidentified variability by the one-common-trend DFM selected above, explanatory variables were introduced into the analysis. The DFMs that were evaluated using different combinations of explanatory variables and

common trends are given in Table 2. The three explanatory variables used were the  $ET_p^*$ ,  $(pP + DP)^*$ , and  $DF^*$  time series that correspond with the original time series shown in Fig. 2a to 2c. Disaggregating the water output and inputs across the soil surface into the three separate terms [ $ET_p^*$ ,  $(pP + DP)^*$ , and  $DF^*$ ] permitted evaluation of the individual contribution of each explanatory variable to the soil water status temporal dynamics.

The number of common trends and performance coefficients for these explanatory-variable models are given in Table 2. Based on the different  $C_{\text{eff}}$  and AICs obtained, the best DFM (AIC = 5691,  $C_{\text{eff}} = 0.720$ ) included one common trend and the three explanatory variables [ $ET_p^*$ ,  $(pP + DP)^*$ , and  $DF^*$ ]. By introducing explanatory variables into the DFM, one may expect a reduction in the importance of the common trend (lower  $\rho_{1,n}$ ) or an improvement in the goodness of fit. The left panel in Fig. 6a illustrates this common trend, while the corresponding canonical correlation coefficients ( $\rho_{1,n}$ ) are shown in the right panel. The trend is similar to that obtained when the explanatory variables

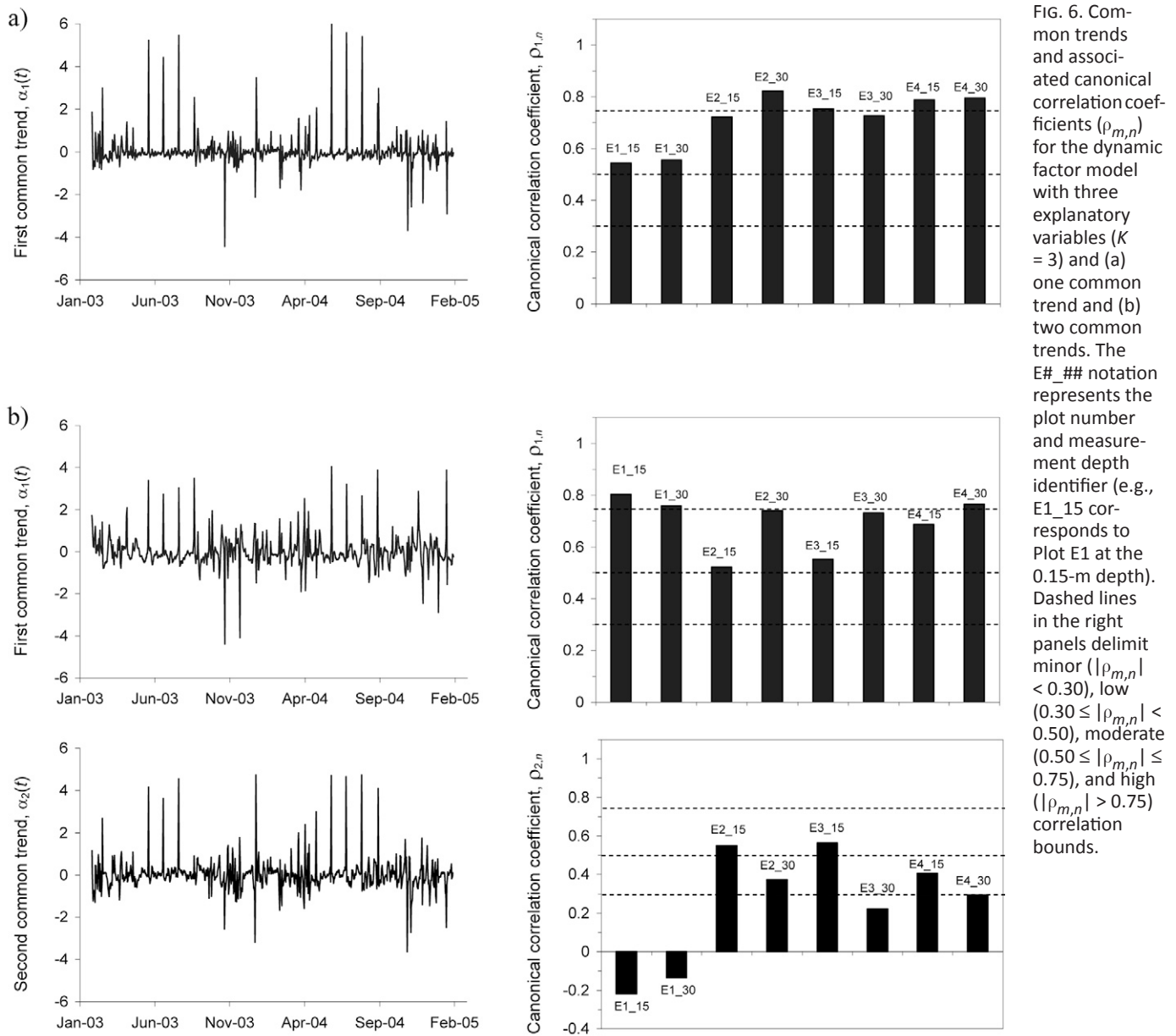


FIG. 6. Common trends and associated canonical correlation coefficients ( $\rho_{m,n}$ ) for the dynamic factor model with three explanatory variables ( $K = 3$ ) and (a) one common trend and (b) two common trends. The E#\_## notation represents the plot number and measurement depth identifier (e.g., E1\_15 corresponds to Plot E1 at the 0.15-m depth). Dashed lines in the right panels delimit minor ( $|\rho_{m,n}| < 0.30$ ), low ( $0.30 \leq |\rho_{m,n}| < 0.50$ ), moderate ( $0.50 \leq |\rho_{m,n}| \leq 0.75$ ), and high ( $|\rho_{m,n}| > 0.75$ ) correlation bounds.

were not included in the DFA (Fig. 5a), but the lower magnitude of  $\rho_{1,n}$  indicates that the influence of this common trend on each of the eight response time series decreased when hydrologic flux information was included in the DFM (cf. Fig. 5a and 6a). In addition, the DFM that included the three hydrologic explanatory variables ( $K = 3$ ) yielded a  $C_{\text{eff}}$  (0.720) that was similar to that for the  $K = 0$  DFM (0.717). Therefore the common trend in Fig. 5a, which represents the total variability observed in the soil refractive index time series, can be split into the contribution of the hydrologic fluxes plus the remaining unexplained variability represented by the common trend in Fig. 6a. In other words, by including the hydrologic explanatory variables into the DFM, we have managed to reduce the unexplained variability described by Fig. 5a. This conclusion is not constrained to considering one single trend ( $M = 1$ ) but is also valid for  $M = 2$  (cf. Fig. 5b and 6b, Table 2). Hence, both the first and second trends in Fig. 5b contain information already described by the hydrologic fluxes.

The DFA provides regression coefficients ( $\beta_{k,n}$ ) for each explanatory hydrologic variable. Since the explanatory variables

were standardized, the corresponding  $\beta_{k,n}$  quantify their relative importance within the DFM (Zuur et al., 2003b). Figure 7 shows the regression coefficients used for modeling  $\Delta\sqrt{\epsilon}^*$  at both monitoring depths and at the four plots. Both  $\text{ET}_p^*$  and  $(\text{pP} + \text{DP})^*$  were found to have a significant ( $t$  value  $> 2$ ) influence on the eight response time series. According to Fig. 7a and 7b, the regression coefficients  $\beta_{(\text{pP} + \text{DP})^*,n}$  are in general higher than  $\beta_{\text{ET}_p^*,n}$ , indicating that the contribution of rainfall to the temporal dynamics of  $\sqrt{\epsilon}$  within the watershed is larger than the effect of potential evapotranspiration. Regarding the particular influence of these hydrologic variables on the individual  $\Delta\sqrt{\epsilon}^*$  time series for each plot, the higher  $\beta_{(\text{pP} + \text{DP})^*,n}$  values corresponding to 0.15 m suggest that  $(\text{pP} + \text{DP})^*$  is relatively more important for describing  $\Delta\sqrt{\epsilon}^*$  at the upper monitoring depth at Plots E2, E3, and E4 than it is at Plot E1 (Fig. 7b). In contrast, the  $\beta_{\text{ET}_p^*,n}$  values indicate no consistent influence of  $\text{ET}_p^*$  on soil water status within or among depths and plot locations (Fig. 7a). This is not surprising, since the approach followed in this analysis (limited by the available information) does not consider that plant

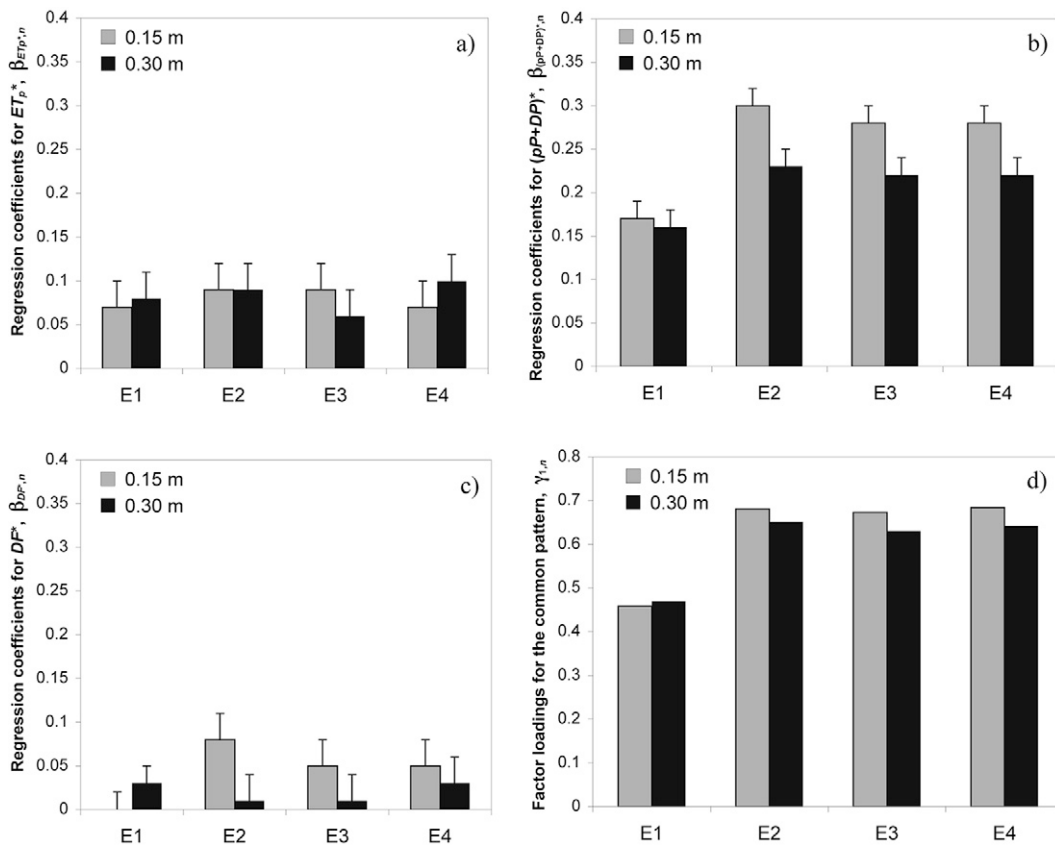


FIG. 7. Regression coefficients (in absolute value) and common-trend factor loadings for the dynamic factor model (DFM) selected as the best daily change in the deseasonalized soil refractive index ( $\Delta\sqrt{\varepsilon^*}$ ) time series model for each field plot (E1–E4) and depth (0.15 and 0.30 m). Shown are regression coefficients for (a) deseasonalized potential evapotranspiration,  $ET_p^*$ ; (b) standardized through-fall plus canopy drip,  $(pP + DP)^*$ ; and (c) standardized intercepted fog-water drip,  $DF^*$ ; as well as (d) the factor loadings ( $\gamma_{1,n}$ ).

water uptake may be satisfied by deeper soil moisture and root uptake below the upper 0.30-m depth that was monitored in this study. Finally, the low and nonsignificant regression coefficients  $\beta_{DF^*,n}$  indicate a negligible effect of intercepted fog water on the response time series (Fig. 7c). Such a small contribution of fog drip from the canopy is in agreement with results of Ritter et al. (2008), who studied the importance of the water supplied by wind-driven fogs in the same forest watershed using aboveground meteorological data and a physically based impaction model. This is not to say that fog is not relevant, since its presence may limit tree transpiration by reducing global radiation, vapor-pressure deficit, and air temperature (Burgess and Dawson, 2004; Ritter et al., 2009).

The factor loadings  $\gamma_{1,n}$  for each plot and depth are shown in Fig. 7. The magnitude and sign of  $\gamma_{1,n}$  determine how the common trend (Fig. 6a) is related to the original time series within the best ( $M = 1, K = 3$ ) DFM. Both the  $\gamma_{1,n}$  and  $\beta_{k,n}$  are weighing coefficients within the DFM (see Eq. [14]) and, because the time series were standardized, they may be compared. Compared with the regression coefficients discussed above (Fig. 7a–7c), the higher  $\gamma_{1,n}$  values for all plots and monitoring depths (Fig. 7d) indicate that the weight of the common trend within the DFM is important. We may thus conclude that the information accounted by the hydrologic fluxes included in the DFM represents only part of the total unexplained variability (common trend in Fig. 5a) in the observed soil water dynamics. This means that part of the information contained in this common trend remains unexplained and the three selected hydrologic fluxes alone do not completely describe the changes in soil water status.

In addition to the above discussion based on the interpretation of the DFA results, the performance of the DFM may also

be evaluated by extrapolating the best ( $M = 1, K = 3$ ) DFM to the original data set (Fig. 2d). To extrapolate the selected DFM to the original data set,  $C_{\text{eff}}$  were computed from the measured and fitted response  $\sqrt{\varepsilon}$  time series, instead of  $\Delta\sqrt{\varepsilon^*}$ . For this purpose, the fitted  $\Delta\sqrt{\varepsilon^*}$  values obtained with the best DFM were back-transformed to  $\sqrt{\varepsilon^*}$  values and then again to  $\sqrt{\varepsilon}$  (see Fig. 4). In general, the  $C_{\text{eff}}$  for the eight original soil water status time series ranged from 0.818 to 0.924 and indicated that the selected DFM successfully predicted the observed temporal variability in topsoil water status within the forest watershed. It is noted that the back-transformation implies an improvement in the goodness of fit for the untransformed data series relative to that reported for the best ( $M = 1, K = 3$ ) DFM that used the  $\Delta\sqrt{\varepsilon^*}$  data series ( $C_{\text{eff}} = 0.717$ ). This result stresses the importance of the seasonal component in the temporal dynamics of the soil refractive index.

## Conclusions

Detailed hydrologic, multivariate, time-dependent data sets of soil water status (expressed in terms of the TDR soil refractive index) in the topsoil of a forest watershed were studied using DFA. First, the analysis served to successfully identify a single trend common to all observed time series monitored at two depths and at four locations within the watershed. The resulting DFM, based on such a common trend, described satisfactorily each of these temporal data sets. This trend represents the unexplained variability common to each of the eight time series and it may be viewed as a black box that accounts for all the factors and processes involved in the soil water dynamics (e.g., soil properties, physical and biological processes, etc.). Second, the inclusion of selected hydrologic fluxes (forest potential evapotranspiration, rainfall, and fog drip) as explanatory variables in the DFA resulted in lower

canonical correlation coefficients and, therefore, a reduction in the unexplained variability in the observed data. Evaluation of the DFM regression coefficients showed that the rainfall contribution to the soil surface (throughfall plus canopy dripping) and, to a lesser extent, forest potential evapotranspiration were the predominant variables that described temporal changes in the soil water status. Compared with the rainfall contribution, regression coefficients for intercepted fog water dripping from the canopy were one order of magnitude lower, and indicated a negligible direct effect of fog water on the soil water dynamics. Nonetheless, fog may have an indirect effect on soil water depletion because its presence can lower the evaporative demand and, in turn, reduce evapotranspiration. It was demonstrated that using DFA, the complex variability in multivariate hydrologic time series could be simplified by a regression method without the need of a priori detailed information about site-specific characteristics such as soil properties, vegetation cover, etc. Finally, DFA may be considered a useful scaling technique, whereby a (single) common trend, together with spatially dependent regression parameters, allowed us to reproduce time series sampled at different locations within the watershed.

#### ACKNOWLEDGMENTS

This work was financed with funds of the INIA-Programa Nacional de Recursos y Tecnologías Agroalimentarias (Project RTA2005-228). A. Ritter acknowledges financial help from the European Social Fund. We would like to thank Thomas Keller (Up GmbH, Germany) for his support with the field instrumentation, and Dr. Guido Aschan (University of Duisburg-Essen) for collaborating on the installation of the sap flow measurement system. We also thank A. Fernández and L.A. Gómez (Garajonay National Park) for their support. We wish to acknowledge the collaboration between the Spanish Unsaturated Zone Studies Group (ZNS) and the Unsaturated Zone Interest Group (UZIG) that made possible the inclusion of this work in this special collection.

#### References

- Aboal, J. 1998. Los flujos netos hidrológicos y químicos asociados de un bosque de laurisilva en Tenerife. (In Spanish.) Ph.D. diss. Available at dialnet.unirioja.es/servlet/tesis?codigo=637 (verified 16 Feb. 2009). Univ. of La Laguna, La Laguna, Spain.
- Aboal, J., D. Morales, J.M. Hernández, and M.S. Jiménez. 1999. The measurement and modelling of the variation of stemflow in a laurel forest in Tenerife, Canary Islands. *J. Hydrol.* 221:161–175.
- ADC BioScientific Ltd. 2004. LCpro+ portable photosynthesis system: Instruction manual. ADC BioScientific Ltd., Hoddesdon, UK.
- Akaike, H. 1974. A new look at the statistical model identification. *IEEE Trans. Automat. Control* 19:716–723.
- Allen, R.G., L.S. Pereira, D. Raes, and M. Smith. 1998. Crop evapotranspiration: Guidelines for computing crop water requirements. *Irrig. Drain. Pap.* 56. FAO, Rome.
- Aschan, G. 1998. Mikroklima, Energiebilanz, und Wasserhaushalt von tropischen und extratropischen Wäldern. *Biol. Ser.* 159. (In German.) Tectum-Verlag, Marburg, Germany.
- Aschan, G., M.S. Jiménez, D. Morales, and R. Löscher. 1994. Aspectos microclimáticos de un bosque de laurisilva en Tenerife. (In Spanish.) *Vieraea* 23:125–141.
- Bruckner, A., E. Kandeler, and C. Kampichler. 1999. Plot-scale spatial pattern of soil water content, pH, substrate induced respiration and N mineralisation in a temperate coniferous forest. *Geoderma* 93:207–223.
- Brutsaert, W. 1975. Comments on surface roughness parameters and the height of dense vegetation. *J. Meteorol. Soc. Jpn.* 53:96–97.
- Burgess, S.S.O., and T.E. Dawson. 2004. The contribution of fog to the water relations of *Sequoia sempervirens* (D. Don): Foliar uptake and prevention of dehydration. *Plant Cell Environ.* 27:1023–1034.
- Dempster, A.P., N.M. Laird, and D.B. Rubin. 1977. Maximum likelihood from incomplete data via the EM algorithm. *J.R. Stat. Soc. Ser. B* 39:1–38.
- Dingman, L. 2002. *Physical hydrology*. Prentice Hall, Upper Saddle River, NJ.
- Ferré, P.A., D.L. Rudolph, and R.G. Kachanoski. 1996. Spatial averaging of water content by time domain reflectometry: Implications for twin rod probes with and without dielectric coatings. *Water Resour. Res.* 32:271–279.
- Gash, J.H.C., and A.J. Morton. 1978. An application of the Rutter model to the estimation of the interception loss from Theford forest. *J. Hydrol.* 38:49–58.
- Geweke, J.F. 1977. The dynamic factor analysis of economic time series models. p. 365–382. *In* D.J. Aigner and A.S. Goldberger (ed.) *Latent variables in socio-economic models*. North-Holland, Amsterdam.
- Golubic, I. 2001. Vegetationskundliche Analyse von Lorbeerwald- und ähnlichen Beständen im Rahmen einer Untersuchung des Landschaftswasserhaushalts im Garajonay Nationalpark La Gomera (Kanarische Inseln). (In German.) Diploma thesis. Univ. of Essen, Essen, Germany.
- Granier, A. 1985. Une nouvelle méthode pour la mesure des flux de sève dans le tronc des arbres. (In French.) *Ann. Sci. For.* 42:193–200.
- Harvey, A.C. 1989. *Forecasting, structural time series models and the Kalman filter*. Cambridge Univ. Press, New York.
- Jarvis, P.G. 1976. The interpretation of leaf water potential and stomatal conductance found in canopies in the field. *Philos. Trans. R. Soc. London Ser. B* 273:593–610.
- Jiménez, M.S., N. Nadezhdina, J. Čermák, and D. Morales. 2000. Radial variation in sap flow in five laurel forest tree species in Tenerife, Canary Islands. *Tree Physiol.* 20:1149–1156.
- Jiménez Mendoza, C.C., M.L. Tejedor Salguero, A. Rodríguez Rodríguez, and E. Fernández Caldas. 1990. Los suelos del Parque Nacional de Garajonay y su entorno. (In Spanish.) p. 46–55. *In* P.L. Pérez de Paz (ed.) *Parque Nacional de Garajonay, Patrimonio Mundial*. Excmo. Cabildo Insular de La Gomera, ICONA, La Gomera, Spain.
- Leyton, L., R.C. Reynolds, and F.B. Thompson. 1967. Rainfall interception in forest and moorland. p. 163–179. *In* W.E. Sopper and H.W. Lull (ed.) *Forest hydrology*. Pergamon Press, Oxford, UK.
- Lhomme, J.-P., E. Elguero, A. Chehbouni, and G. Boulet. 1998. Stomatal control of transpiration: Examination of Monteith's formulation of canopy resistance. *Water Resour. Res.* 34:2301–2308.
- Lütkepohl, H. 1991. *Introduction to multiple time series analysis*. Springer-Verlag, Berlin.
- Mallants, D., B.P. Mohanty, D. Jaques, and J. Feyen. 1996. Spatial variability of hydraulic properties in a multilayered soil profile. *Soil Sci.* 161:167–181.
- Márkus, L., O. Berke, J. Kovács, and W. Urfer. 1999. Spatial prediction of the intensity of latent effects governing hydrogeological phenomena. *Environmetrics* 10:633–654.
- Matthews, E. 1984. Vegetation, land-use and seasonal albedo data sets. Appendix D. *In* Global change data base Africa documentation. NOAA, Natl. Geophys. Data Ctr., Boulder, CO.
- Muñoz-Carpena, R., A. Ritter, and Y.C. Li. 2005. Dynamic factor analysis of groundwater quality trends in an agricultural area adjacent to Everglades National Park. *J. Contam. Hydrol.* 80:49–70.
- Nash, J.E., and J.V. Sutcliffe. 1970. River flow forecasting through conceptual models: Part 1-A. Discussion of principles. *J. Hydrol.* 10:282–290.
- Philip, J.R. 1991. Soils, natural science, and models. *Soil Sci.* 151:91–98.
- Raat, K.J., G.P.J. Draaijers, M.G. Schaap, A. Tietema, and J.M. Verstraten. 2002. Spatial variability of throughfall water and chemistry and forest floor water content in a Douglas fir forest stand. *Hydrol. Earth Syst. Sci.* 6:363–374.
- Regalado, C.M., and A. Ritter. 2006. Geostatistical tools for characterizing the spatial variability of soil water repellency parameters in a laurel forest watershed. *Soil Sci. Soc. Am. J.* 70:1071–1081.
- Regalado, C.M., and A. Ritter. 2007. An alternative method to estimate zero flow temperature differences for Granier's thermal dissipation technique. *Tree Physiol.* 27:1093–1102.
- Regalado, C.M., A. Ritter, and R. Becker. 2006. Comments on "Monitoring soil water content profiles with a commercial TDR system: Comparative field tests and laboratory calibration." *Vadose Zone J.* 5:1067–1068.
- Ritter, A., and R. Muñoz-Carpena. 2006. Dynamic factor modeling of ground and surface water levels in an agricultural area adjacent to Everglades National Park. *J. Hydrol.* 317:340–354.
- Ritter, A., R. Muñoz-Carpena, D.D. Bosch, B. Schaffer, and T.L. Potter. 2007. Agricultural land use and hydrology affect variability of shallow groundwater nitrate concentration in South Florida. *Hydrol. Processes* 21:2464–2473.
- Ritter, A., C.M. Regalado, and G. Aschan. 2008. Fog water collection in a subtropical elfin laurel forest of the Garajonay National Park (Canary Islands):

- A combined approach using artificial fog catchers and a physically-based impaction model. *J. Hydrometeorol.* 9:920–935.
- Ritter, A., C.M. Regalado, and G. Aschan. 2009. Fog reduces transpiration in tree species of the Canarian relict heath-laurel cloud forest (Garajonay National Park, Spain). *Tree Physiol.* 29:517–528.
- Rodríguez Rodríguez, A., C.D. Arbelo, J.A. Guerra, J.L. Mora, J.S. Notario, and C.M. Armas. 2006. Organic carbon stocks and soil erodibility in Canary Islands Andosols. *Catena* 66:228–235.
- Rutter, A.J., K.A. Kershaw, P.C. Robins, and A.J. Morton. 1971. A predictive model of rainfall interception in forests: 1. Derivation of the model from observations in a plantation of Corsican pine. *Agric. For. Meteorol.* 9:367–384.
- Rutter, A.J., A.J. Morton, and P.C. Robins. 1975. A predictive model of interception loss in forests: II. Generalization of the model and comparison with observations in some coniferous and hardwood stands. *J. Appl. Ecol.* 12:367–380.
- Salas, J.D. 1993. Analysis and modeling of hydrologic time series. p. 19.1–19.72. *In* D.R. Maidment (ed.) *Handbook of hydrology*. McGraw-Hill, New York.
- Santana Pérez, L. 1990. La importancia hidrológica de las nieblas en las cumbres del Parque Nacional de Garajonay. (In Spanish.) p. 66–71. *In* P.L. Pérez de Paz (ed.) *Parque Nacional de Garajonay, Patrimonio Mundial*. Excmo. Cabildo Insular de La Gomera, ICONA, La Gomera, Spain.
- Schaap, M.G., W. Bouten, and J.M. Verstraten. 1997. Forest floor water content dynamics in a Douglas fir stand. *J. Hydrol.* 201:367–383.
- Schume, H., G. Jost, and K. Katzensteiner. 2003. Spatio-temporal analysis of the soil water content in a mixed Norway spruce (*Picea abies* (L.) Karst.)–European beech (*Fagus sylvatica* L.) stand. *Geoderma* 112:273–287.
- Shumway, R.H., and D.S. Stoffer. 1982. An approach to time series smoothing and forecasting using the EM algorithm. *J. Time Ser. Anal.* 3:253–264.
- Soil Survey Staff. 1999. *Soil Taxonomy: A basic system of soil classification for making and interpreting soil surveys*. 2nd ed. U.S. Gov. Print. Office, Washington, DC.
- Stewart, J.B. 1988. Modelling surface conductance of pine forest. *Agric. For. Meteorol.* 43:19–37.
- Thissen, B. 2001. Untersuchung zur Abschätzung des Einfluss des Bodens auf die Wasserbilanz von Teilflächen des Garajonay Nationalparks, La Gomera, Spanien. (In German.) Diploma thesis. Univ. of Essen, Essen, Germany.
- Thom, A.S. 1971. Momentum absorption by vegetation. *Q.J.R. Meteorol. Soc.* 97:414–428.
- Thom, A.S. 1975. Momentum, mass, and heat exchange. p. 57–109. *In* J.L. Monteith (ed.) *Vegetation and the atmosphere*. Academic Press, San Diego.
- Thom, A.S., and H.R. Oliver. 1977. On Penman's equation for estimating regional evaporation. *Q.J.R. Meteorol. Soc.* 103:345–357.
- van Dijk, A.I.J.M., and L.A. Bruijnzeel. 2001. Modelling rainfall interception by vegetation of variable density using an adapted analytical model: 1. Model description. *J. Hydrol.* 247:230–238.
- Wallis, M.G., and D.J. Horne. 1992. Soil water repellency. *Adv. Soil Sci.* 20:91–146.
- Warkentin, B.P., and T. Maeda. 1980. Physical and mechanical characteristics of Andisols. p. 281–299. *In* B.K.G. Theng (ed.) *Soils with variable charge*. New Zealand Soc. Soil Sci., Lower Hutt.
- Wu, L.S.-Y., J.S. Pai, and J.R.M. Hosking. 1996. An algorithm for estimating parameters of state-space models. *Stat. Prob. Lett.* 28:99–106.
- Zuur, A.F., R.J. Fryer, I.T. Jolliffe, R. Dekker, and J.J. Beukema. 2003a. Estimating common trends in multivariate time series using dynamic factor analysis. *Environmetrics* 14:665–685.
- Zuur, A.F., E.N. Ieno, and G.M. Smith. 2007. *Analysing ecological data*. Springer-Verlag, Berlin.
- Zuur, A.F., and G.J. Pierce. 2004. Common trends in Northeast Atlantic squid time series. *J. Sea Res.* 52:57–72.
- Zuur, A.F., I.D. Tuck, and N. Bailey. 2003b. Dynamic factor analysis to estimate common trends in fisheries time series. *Can. J. Fish. Aquat. Sci.* 60:542–552.